Crossover from one to two dimensions in liquid ^{4}He in a nanopore

L. Vranješ Markić [1,*], Krešimir Dželalija [1], and H. R. Glyde [2]

[1]*Faculty of Science, University of Split, HR-21000 Split, Croatia, European Union*
[2]*Department of Physics and Astronomy, University of Delaware, Newark, Delaware 19716-2593, USA*

Using diffusion and path-integral Monte Carlo methods, we show that liquid ^{4}He confined in a narrow nanopore of liquid radius $R = 4$ Å undergoes a crossover from a one-dimensional (1D) to a two-dimensional (2D) fluid as a function of liquid density. At low liquid density, e.g., a linear density $\rho_0 = 0.15$ Å^{-1}, the liquid energy is at a minimum when the liquid lies in a line at the center of the pore. The pair distribution function $g(x)$, the one-body density matrix $n(x)$, and the superfluid fraction ρ_S/ρ_0 all show 1D character that is well described by Luttinger liquid (LL) predictions. As density is increased, there is a crossover to 2D with the minimum energy configuration moving from a line at the center of the pore to a film near the pore walls. At linear density $\rho_0 > 0.40$ Å^{-1}, the ^{4}He lies predominantly in a 2D cylindrical film midway between the center and the nanopore walls. The $g(x)$, $n(x)$, and ρ_S/ρ_0 all show 2D character and the film has a low but finite transition temperature. ^{4}He at a bulk liquid density corresponds to $\rho_0 = 0.6$ Å^{-1} in the pore which lies in the 2D regime.

I. INTRODUCTION

Dimensions play a key role in determining the behavior of quantum systems. Initially, exotic phenomena such as Bose-Einstein condensation (BEC), superfluidity, and superconductivity were formulated and investigated with extensive three-dimensional (3D) systems in mind [1–7]. In 3D Bose quantum liquids, BEC and superfluidity have a common, finite onset temperature [7,8] T_c. Below T_c, the superfluid fraction ρ_S/ρ_0 increases gradually [5,9,10] from zero at T_c to unity at $T = 0$. Similarly, the Bose-Einstein condensate fraction, $n_0 = N_0/N$, increases gradually from zero at T_c to a maximum value ($n_0 \leqslant 1$) at $T = 0$ set by the degree of interboson interaction. The corresponding one-body density matrix (OBDM) $n(r)$ develops a infinitely long tail below T_c, the height of the tail being the condensate fraction.

Interest was soon extended to two-dimensional (2D) systems in which the ordered states and transitions are quite different [11,12]. In 2D, on cooling, ρ_S/ρ_0 jumps from zero to a finite value at T_c [12]. It increases slowly thereafter to $\rho_S/\rho_0 = 1$ at $T = 0$. This discontinuous jump at T_c is rounded in finite-area films [9,10]. At temperatures $T > T_c$, the long-range asymptotic tail of the OBDM $n(r)$ decays exponentially with r. At $T < T_c$ the long-range asymptotic tail decays algebraically, reflecting long-range correlations and can be expressed as $n(r) \sim r^{-\eta(T)}$. At $T > T_c$ but close to T_c, $n(r)$ is also algebraic at intermediate range r, reflecting the onset of local order near T_c. Within Kosterlitz-Thouless [11] theory, T_c can be identified from the OBDM as the temperature at which the exponent $\eta(T)$ reduces to $\eta(T) = 0.25$. At $T = 0$, $\eta \to 0$, and the OBDM is constant as in 3D.

Today there is keen interest in one-dimensional (1D) quantum systems. The low-energy properties of 1D quantum liquids (QLs) are quite unique and well described by Luttinger liquid (LL) theory [13,14]. At finite temperature, ρ_S/ρ_0 is a finite-size effect only. There is no T_c. The ρ_S/ρ_0 scales as a product of LT, the length L of the 1D liquid times the temperature T, rather than independently on L and T. At high density, $n(x)$ and the pair correlation function $g(x)$ develop long-range oscillations characteristic of the atomic order imposed by 1D.

The dimension of a quantum liquid is typically set by its confining boundaries. For example, three-dimensional QLs are found in a container or a nearly spherical confining trap. Two-dimensional QLs are generally created as films on surfaces [15,16] or in a trap where motion is possible in 2D only. The film could be on the internal surface of a nanopore [17] in which case the film has a cylindrical profile. A second or third layer of film can be added which usually shows 2D character [18–21]. One-dimensional QLs can, in principle, be created by confining bosons in very narrow nanopores or in optical lattices in which motion is possible in 1D only. Designing confinement that unambiguously creates a 1D system is not simple. Creating and investigating 1D QLs in nanopores and optical lattices is an exciting and active field of research today, the subject of extensive reviews [14,22,23].

Specifically, path-integral Monte Carlo (PIMC) calculations show that a freestanding 1D line of atoms has a winding number and particle number fluctuations well described by LL theory with minor deviations [24]. Similarly, a line of ^{4}He atoms at the center of small radii nanopores shows [25] correlations consistent with 1D. Superflow is observed in larger radii nanopores where there are 2D shells or layers of ^{4}He in addition to the 1D line [26]. In nanopores in which the radius of the liquid is $R = 3$ Å, ^{4}He unambiguously shows a 1D superfluid fraction and OBDM that is well reproduced by LL theory [27,28]. At larger R where there are 2D layers, the ρ_S/ρ_0, where now ρ_S and ρ_0 are 1D densities, and OBDM show scaling that is consistent with a 2D fluid
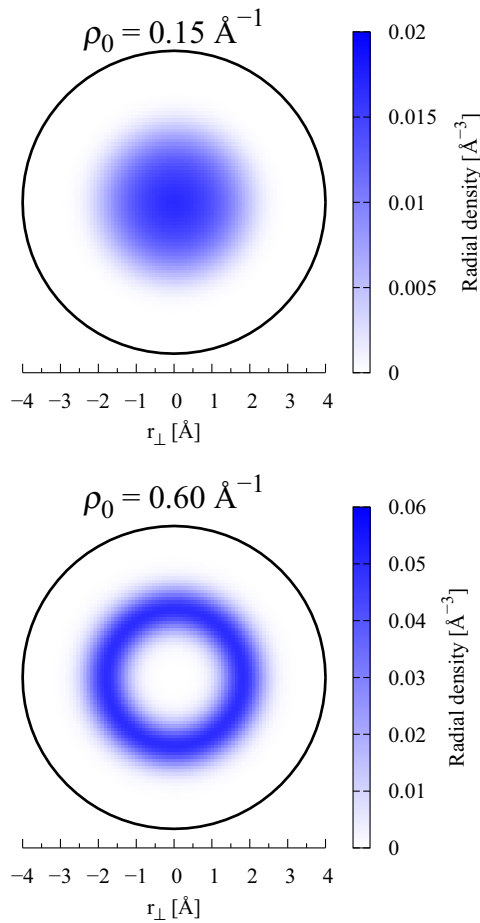
*Corresponding author: leandra@pmfst.hr

FIG. 1. Density distribution of liquid ^{4}He (blue shading) confined in a nanopore of liquid radius $R = 4$ Å. Upper frame: Low linear ^{4}He density, $\rho_0 = N/L = 0.15$ Å^{-1}, where the liquid density lies along a 1D line at the center of the nanopore. Lower frame: High linear ^{4}He density, $\rho_0 = 0.60$ Å^{-1}, where the liquid density is concentrated in a 2D cylindrical shell.

[27]. Calculations find that a 1D line of ^{4}He supports a phonon-roton mode that has a roton energy that goes to zero at modest and higher densities [29,30]. At finite temperature, two sound modes are predicted [31]. A freestanding line of parahydrogen [32,33], p-H$_2$, and p-H$_2$ in nanopores [32,34–37] are similar except that superflow in any dimension has not yet been demonstrated, the goal of many studies. Similarly, spin-polarized H in a reduced dimension has been investigated [38].

In this paper, our goal is to display a transition from 1D to 2D in a quantum liquid without changing the confinement. The crossover from 1D to 2D is made solely by changing the liquid density. Liquid helium confined in a nanopore of radius $R = 4$ Å is considered. At low liquid density the equilibrium configuration is a 1D line of atoms at the center of the nanopore, as shown in the upper frame of Fig. 1. At higher liquid density the equilibrium distribution crosses over to a 2D film near the pore walls, as shown in the lower frame of Fig. 1. At low density the liquid is well described by LL theory. The ρ_S/ρ_0 scales as LT and the OBDM $n(x)$ decays algebraically with long-range oscillations, as expected for a LL. At high

density, however, the $n(x)$ and pair correlation function $g(x)$ do not show long-range oscillations. Rather, $n(x)$ shows a smooth algebraic tail expected for a 2D fluid and a temperature dependence that indicates a finite superfluid transition temperature $T_c \simeq 0.15$–0.2 K in the fluid. The ρ_S/ρ_0 shows finite-size effects consistent with a 2D fluid that has the above T_c. In short, the liquid shows 1D LL behavior at low density and 2D film behavior at high density.

II. MODEL NANOPORES AND HELIUM DISTRIBUTIONS

In a typical nanopore, such as FSM-16 (e.g., diameter, $d = 28$ Å) and MCM-41, the initial ^{4}He entering the nanopore is deposited in layers on the pore walls. The first roughly 1.5 layers of helium (5 Å thick) are amorphous solid ^{4}He layers. The subsequent layers are liquid. A liquid layer may be defined as a 2D region of high liquid density with regions of low density on each side, as depicted in the bottom frame of Fig. 1. In the first few liquid layers, the density at the layer center is much greater than that between layers. After several layers, the density becomes uniform.

The present model of a nanopore is chosen to represent both the nanopore and the $\sim$5-Å-thick solid ^{4}He layers on the pore walls. In this way, only the liquid in the nanopore needs to be simulated. The radius of the model nanopore confining the liquid is chosen as $R = 4$ Å. Taking account of the solid layers this would correspond to an actual nanopore of diameter $d = 18$ Å. The model nanopore is described in detail in Refs. [27,28].

In larger nanopores, at a saturated vapor pressure (SVP), the liquid in the layers and near the center of the pore is at 3D bulk liquid SVP density, $\rho = 0.0218$ Å^{-3} (interatomic spacing $a_0 \simeq 3.7$ Å), or close to it. However, the equilibrium density of a 1D line or 2D film of liquid ^{4}He is significantly less. For example, the equilibrium, zero-pressure linear density ρ_0 of a freestanding line of ^{4}He atoms is [29,30,39] $\rho_0(\text{eq}) = 0.036$ Å$^{-1}(a_0 = 27.8$ Å) with a binding energy [39] of only 1.7 mK. The spinodal density of a 1D line [30,39] is $\rho_0(\text{sp}) = 0.026$ Å^{-1}. Similarly, the equilibrium density of a freestanding 2D ^{4}He film [40,41] is $\rho_{2D}(\text{eq}) = 0.0432$ Å^2 ($a_0 \simeq 5.17$ Å). Thus in small pore nanopores where the ^{4}He has 1D or 2D character we anticipate much lower equilibrium densities than observed in larger nanopores. A pressure must be applied to reach densities found in bulk 3D liquid helium.

III. SIMULATIONS AND CALCULATIONS

The liquid ^{4}He in the nanopore of radius $R = 4$ Å is described by the Hamiltonian,

$$\hat{H} = -\frac{\hbar^2}{2m} \sum_{i=1}^{N} \Delta_i + \sum_{i<j}^{N} U(r_{ij}) + \sum_{i=1}^{N} V(r_{\perp i}). \quad (1)$$

In Eq. (1), N is the number of ^{4}He atoms of mass m, Δ is the Laplacian, $U(r)$ is the ^{4}He interatomic potential represented by the Aziz potential [42], and $V(r_\perp)$ is the confining potential of the nanopore at a distance $r_\perp$ from the center of the nanopore. The nanopore potential $V(r_\perp)$ confining the liquid represents the nanopore itself plus the layers of solid helium on the nanopore walls. The most important feature of the

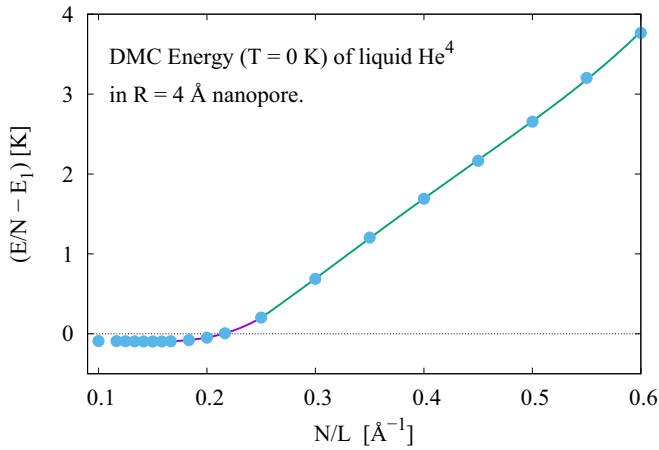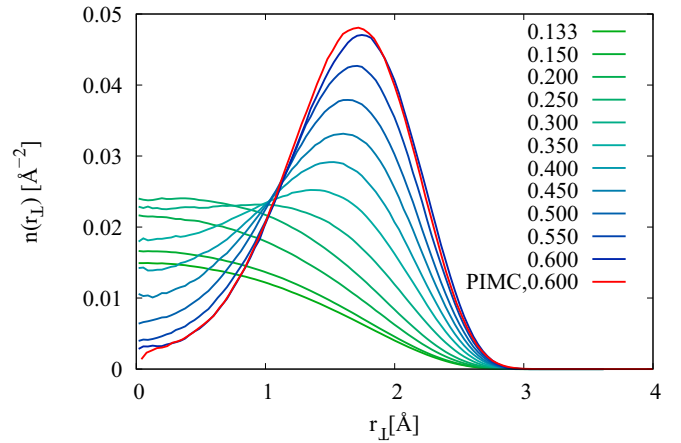FIG. 2. Energy of liquid ^{4}He in a nanopore of liquid radius $R = 4$ Å vs liquid linear density $\rho_0 = N/L$.

FIG. 3. The density profile $n(r_\perp)$ vs the distance $r_\perp$ from the nanopore center of liquid ^{4}He in a nanopore of liquid radius $R = 4$ Å at linear densities $0.133 < \rho_0 < 0.6$ Å^{-1} calculated using DMC except for the one PIMC value indicated. The profiles show a crossover from a liquid density that has a maximum at the pore center (1D) at low linear density to a layerlike (2D) distribution at high density. The crossover takes place at linear density $\rho_0 \simeq 0.30$–0.40 Å^{-1}.

nanopore is the hard wall of the confining potential. Since ^{4}He also has a hard core, the same potential also describes confinement by solid ^{4}He well. The potential $V(r_\perp)$ and the parameters in it are exactly the same as defined and used previously in Refs. [27,28].

The zero-temperature properties of the liquid such as the ground-state energy were calculated using a second-order diffusion Monte Carlo (DMC) method in which the Schrödinger equation written in imaginary time is solved stochastically. The details of the method are given in Ref. [43]. The guiding wave function was as usual constructed as $\Psi = \prod_{i<j} f(r_{ij})\phi(r_{\perp i})$, where $f(r) = \exp[-(b/r)^5]$ and $\phi(r_\perp)$ was the exact single-particle solution in the confining potential $V(r_\perp)$. Pure estimators [44] were used to calculate the pair distribution functions and the density profiles.

Finite-temperature properties such as ρ_S/ρ_0 and the OBDM were calculated using the finite-temperature worm algorithm path-integral Monte Carlo (PIMC) method [10,45]. The values of the discretized imaginary time $\delta\tau$ were the same as used in Ref. [27], i.e., 0.004–0.005 K^{-1}.

IV. RESULTS

Figure 2 shows the ground-state energy E/N versus the liquid linear density $\rho_0 = N/L$ of liquid ^{4}He confined in the present $R = 4$ Å model nanopore. At low density, the ^{4}He is distributed in a line along the nanopore center. E/N has a shallow, broad minimum at linear density $\rho_0(\text{eq}) = 0.15$ Å^{-1}, the equilibrium density. This $\rho_0(\text{eq})$ is larger but similar to that of a freestanding line of ^{4}He atoms quoted in Sec. II above. The $\rho_0(\text{eq})$ is larger in the nanopore apparently because of the motion that is allowed perpendicular to the centerline of the nanopore and the interaction with the pore walls. The minimum energy is $E/N = -95$ mK/atom which is significantly lower than that of a free line of ^{4}He because of the interaction with the pore walls. A larger minimum energy and equilibrium density has been found in other quasi-1D systems, such as ^{4}He inside (5,5) armchair carbon nanotubes [46]. The energy curve ends at the spinodal density, $\rho_0(\text{sp}) = 0.083$ Å^{-1}, where the liquid becomes unstable to droplet formation. Thus the equilibrium density is low, not far from the spinodal density.

At higher linear density, $\rho_0 \geqslant 0.3$ Å^{-1}, the energy increases approximately linearly with ρ_0, which is not expected for the ground-state energy of a single-phase system. The roughly linear increase of the energy with increasing ρ_0 suggests that some other change such as a change in the ^{4}He density profile in the nanopore is taking place. This change is shown in Fig. 3. At low density, $\rho_0 \lesssim 0.25$ Å^{-1}, the ^{4}He distribution in the nanopore peaks along the center of the nanopore. The liquid is 1D with a distribution perpendicular to the pore centerline. At higher density, $\rho_0 \gtrsim 0.25$ Å^{-1}, the peak density moves from a line to a cylindrical shell or layer with a peak density at $\rho \simeq 1.5$–2.0 Å from the pore center. As ρ_0 increases further, the density in the cylindrical shell increases and the density at the pore center decreases. The region of linear E/N vs ρ_0 in Fig. 2 in the range $0.25 \leqslant \rho_0 \leqslant 0.6$ Å^{-1} is the region of density crossover from a 1D line to a 2D cylindrical layer of liquid in the nanopore.

Figure 4 shows the ^{4}He - ^{4}He pair correlation function $g(x)$ in the direction x along the axis of the nanopore as a function of liquid density. At density $\rho_0 = 0.15$ Å^{-1}, $g(x)$ shows the character expected for a 1D liquid in the nanopore. The $g(x)$ is zero at small x over approximately a hard-core diameter and has modest oscillations expected for a low density in 1D liquid. The oscillations extend to somewhat larger distances as the linear density increases (to $\rho_0 = 0.25$ Å^{-1}). These long-range oscillations are characteristic of 1D at somewhat higher density. As the linear density increases further ($\rho_0 \gtrsim 0.35$ Å^{-1}) and the density distribution is in a 2D layer, the corresponding $g(x)$ is no longer nearly zero at $x \to 0$, as it was for a 1D line of atoms along the nanopore axis.

From the above results, we anticipate that the liquid confined to the $R = 4$ Å nanopore will respond as a 1D liquid at low densities, up to $\rho_0 \simeq 0.25$–0.30 Å^{-1}, and as a 2D liquid layer at higher densities. For low densities up to $\rho_0 = 0.25$ Å^{-1}, Fig. 5 shows the LL parameter, $K \equiv (v_J/v_N)^{1/2} = [\pi^2(\hbar^2/m)\rho_0^3\kappa]^{1/2}$, where m is the mass and κ is the
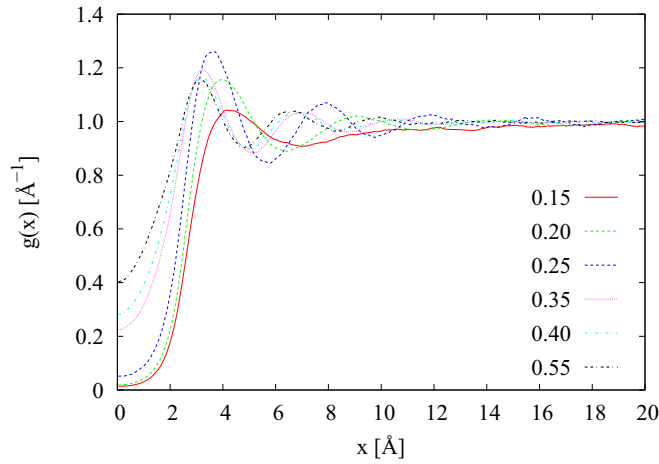
FIG. 4. The pair distribution function $g(x)$ of liquid ^{4}He along the axis of a nanopore of radius $R = 4$ Å at linear densities $0.15 \geqslant \rho_0 \geqslant 0.55$ Å^{-1}. At low linear density $g(x)$ is small out to $x \lesssim 2$ Å, as expected for a 1D liquid. At high density $g(x)$ is finite at $x \to 0$, as expected for 2D cylindrical filling of the pore as shown in the bottom frame of Fig. 1.

compressibility of the 1D liquid. K shows the behavior expected for a 1D liquid, such as found previously [28] in a narrower nanopore where the liquid is 1D at all densities.

Similarly, Fig. 6 shows PIMC calculations of the superfluid fraction ρ_S/ρ_0 at several densities. Also shown as a line are fits of the Luttinger liquid expression for ρ_S/ρ_0 to the PIMC values. At densities up to $\rho_0 = 0.30$ Å^{-1}, the PIMC ρ_S/ρ_0 are well described by the 1D LL theory. The PIMC ρ_S/ρ_0 scale as LT, the product of the pore length L and temperature T, as expected for a 1D liquid. The LL expression for ρ_S/ρ_0 fits well the PIMC calculations of ρ_S/ρ_0. In the fit, the parameter v_J in
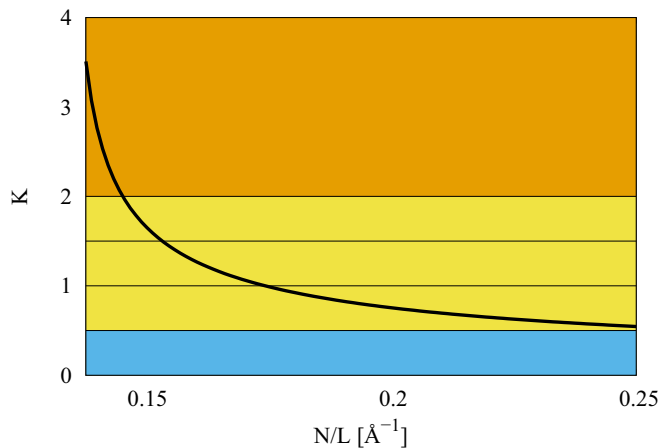

FIG. 5. Luttinger liquid parameter K of liquid ^{4}He in a nanopore of radius $R = 4$ Å as a function of linear density $\rho_0 = N/L$ at low linear density where the liquid is 1D. K is calculated from the ground-state energy, $e = E/N$, as $K = (v_J^0/v_N)^{1/2} = [\pi^2(\frac{\hbar^2}{m})\rho_0^3\kappa]^{1/2}$, where κ is the compressibility, $\kappa^{-1} = \rho_0\partial[\rho_0^2\partial e/\partial\rho_0]/\partial\rho_0$. The superfluidity in the 1D liquid is expected to be robust to a periodic potential for $K > 2$, robust in the presence of disorder for $K > 3/2$, and for $K < 1/2$ the 1D liquid is expected to be quasisolidlike.

LL theory [13] is treated as a free parameter. The fit has a low χ^2 and the best-fit value of v_J agrees well with the value $v_J = v_J^0 = \pi(\hbar/m)\rho_0$ expected for a uniform 1D LL. However, at higher densities, $\rho_0 \geqslant 0.33$ Å^{-1}, the 1D LL theory does not fit the PIMC ρ_S/ρ_0 at all well, suggesting that the liquid is no longer 1D at higher densities. At $\rho_0 = 0.6$ Å^{-1} the ρ_S/ρ_0 clearly does not scale as LT and it is therefore not possible to obtain a fit of the LL expression to the PIMC ρ_S/ρ_0. In Fig. 6 showing $\rho_0 = 0.6$ Å^{-1}, we have simply plotted the LL prediction as a line, with v_J set at $v_J = v_J^0$. Clearly the line does not reproduce the PIMC ρ_S/ρ_0 at all L as it should if the system is 1D. However, it is interesting that the agreement is better at larger L, suggesting that the ^{4}He at high density in the nanopore might approach 1D in the special case of $L \to \infty$.

To further clarify the effective dimensions of the liquid in the present $R = 4$ Å radius nanopore at higher density, we compare in Fig. 7 the OBDM $n(x)$ and pair correlation function $g(x)$ with those found previously in an $R = 3$ Å nanopore. In the $R = 3$ Å nanopore the liquid is definitely 1D at all densities investigated. We compare the two nanopores when the 3D liquid density $\rho' \equiv \pi L(R - 1)^2 = 0.0212$ Å^{-3} is the same in both nanopores and close to the bulk liquid density $\rho = 0.0218$ Å^{-3}. The upper frame of Fig. 7 shows the OBDM. In the present $R = 4$ Å nanopore, $n(x)$ has a flat algebraic long-range tail without oscillations, as expected in a 2D fluid. In the $R = 3$ Å nanopore, $n(x)$ decays more steeply at long range and has long-range oscillations, as expected for 1D. Similarly, in the lower frame, the $g(x)$ in the present $R = 4$ Å pore has only short-range oscillations, as expected for a 2D fluid. In contrast, the liquid in the $R = 3$ Å nanopore has long-range oscillations, as predicted by LL theory for 1D. Thus at higher densities $n(x)$ and $g(x)$ of ^{4}He in the present $R = 4$ Å nanopore show 2D character.

Figure 8 shows $n(x)$ of the liquid in the present $R = 4$ Å nanopore at temperature $T = 0.3$ K at four liquid densities from $\rho_0 = 0.20$ Å^{-1} to $\rho_0 = 0.40$ Å^{-1}. We expect the liquid to be 1D at low densities up to $\rho_0 \simeq 0.30$ Å^{-1}. At low ρ_0, the $n(x)$ in Fig. 8 has a steep algebraic tail, as anticipated for 1D. It shows a crossover from 1D-like at $\rho_0 = 0.20$ and 0.25 Å^{-1} to 2D character at 0.30 and 0.40 Å^{-1}. At the higher densities, the height of the tail is higher and the tail is flatter, as anticipated for a 2D liquid.

To pursue the OBDM further, we recall that in a 2D fluid the transition from the normal to superfluid phase is at a finite temperature T_c. Within Kosterlitz-Thouless theory for a 2D liquid, this T_c can be identified from the OBDM $n(x)$ as the temperature at which the exponent $\eta(T)$ describing the algebraic tail of the OBDM reaches the value $\eta = 0.25$. Figure 9 shows PIMC values of the OBDM as a function of temperature of liquid ^{4}He at a linear density $\rho_0 = 0.40$ Å^{-1}, which is in the 2D density range. The function $n(x) \sim x^{-\eta(T)}$ is fitted to the PIMC values of $n(x)$ in the range $10 \leqslant x \leqslant 25$ Å. In this intermediate range of x, we anticipate that $n(x)$ will decay algebraically with x at temperatures above T_c but close to T_c. The long-range part cannot be used because it is not expected to be algebraic and is affected by the periodic boundary conditions in the present calculations. From the fits, we see that a best fit $\eta = 0.25$ is reached at a finite temperature so that there is finite T_c, as expected for 2D. A $T_c \simeq 0.15$–0.20 K is indicated. This shows that there is a

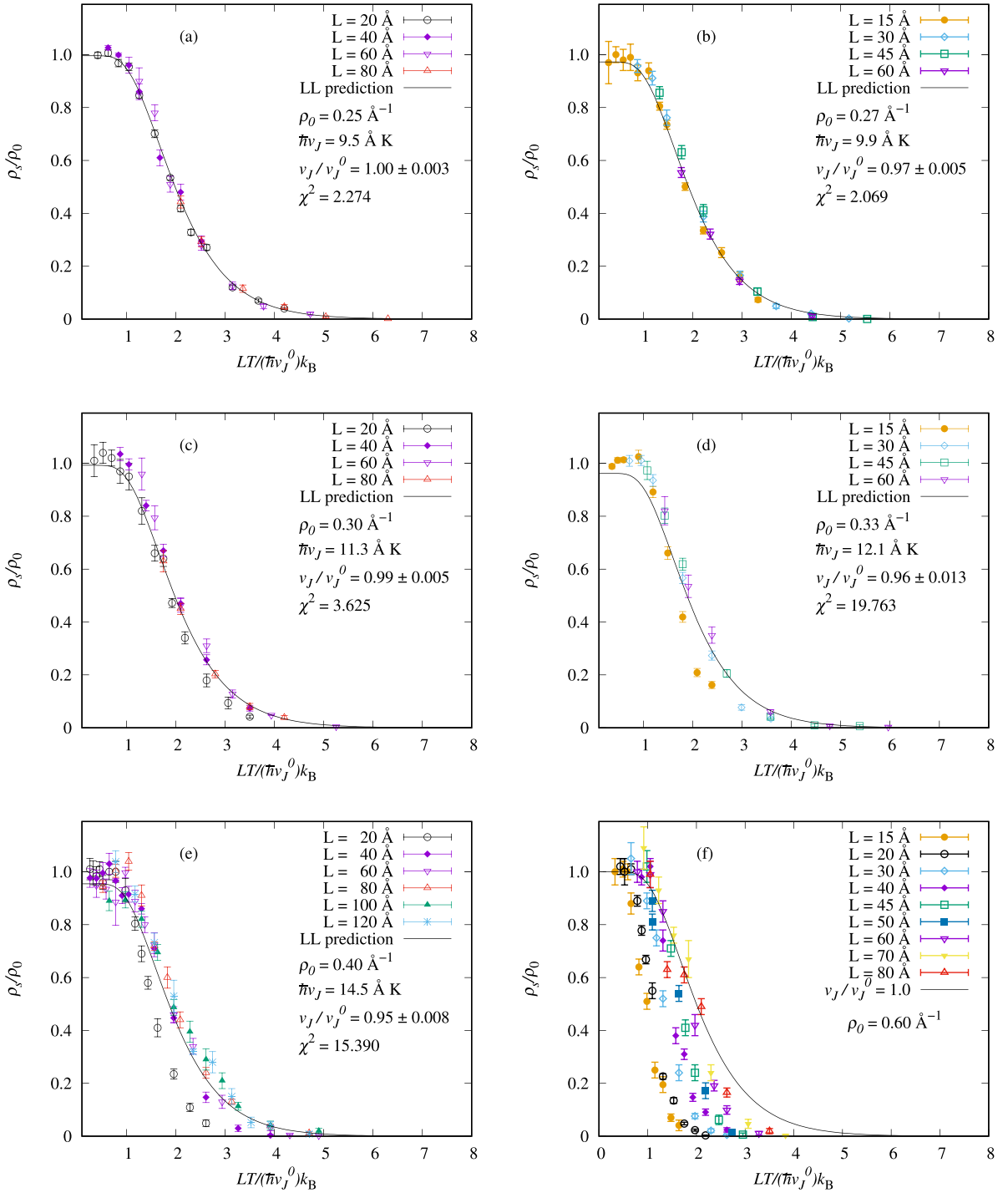FIG. 6. Superfluid fraction ρ_S/ρ_0 of liquid ^{4}He in a nanopore of liquid radius $R = 4$ Å at linear liquid densities between $\rho_0 = 0.25$ and 0.60 Å^{-1}. At low densities up to $\rho_0 = 0.30$ Å^{-1}, the liquid is 1D-like and ρ_S/ρ_0 is well described by LL predictions. A fit of the LL prediction to data has a low χ^2 and ρ_S/ρ_0 scales as $L/\hbar\beta v_J^0 = LT/(\hbar^2/k_B m)\pi\rho_0$. At $\rho_0 = 0.4$ and 0.6 Å^{-1} the liquid is 2D-like and a fit of the LL prediction to data has a large χ^2.

low but finite T_c, as expected for 2D liquid at density $\rho_0 = 0.40$ Å^{-1}. Thus the liquid at higher density has a OBDM and a finite T_c, as expected for a 2D liquid. In contrast, the ρ_S/ρ_0 at lower densities $\rho_0 \lesssim 0.30$ has a OBDM and a ρ_S/ρ_0 well described by 1D LL theory.

In addition to the T_c above obtained from the OBDM, T_c can also be estimated from ρ_S/ρ_0 using scaling methods.

Following Ceperley and Pollock [40], we use the Kosterlitz-Thouless recursion relations to obtain ρ_S/ρ_0 for an infinitely long ($L \to \infty$) film from the present PIMC ρ_S/ρ_0 calculated for finite-length films. Essentially the KT recursion relations are integrated up to a finite length L and fitted to the present PIMC ρ_S/ρ_0 for the corresponding L to obtain unknown parameters in the KT recursion relations. Given the parameters,
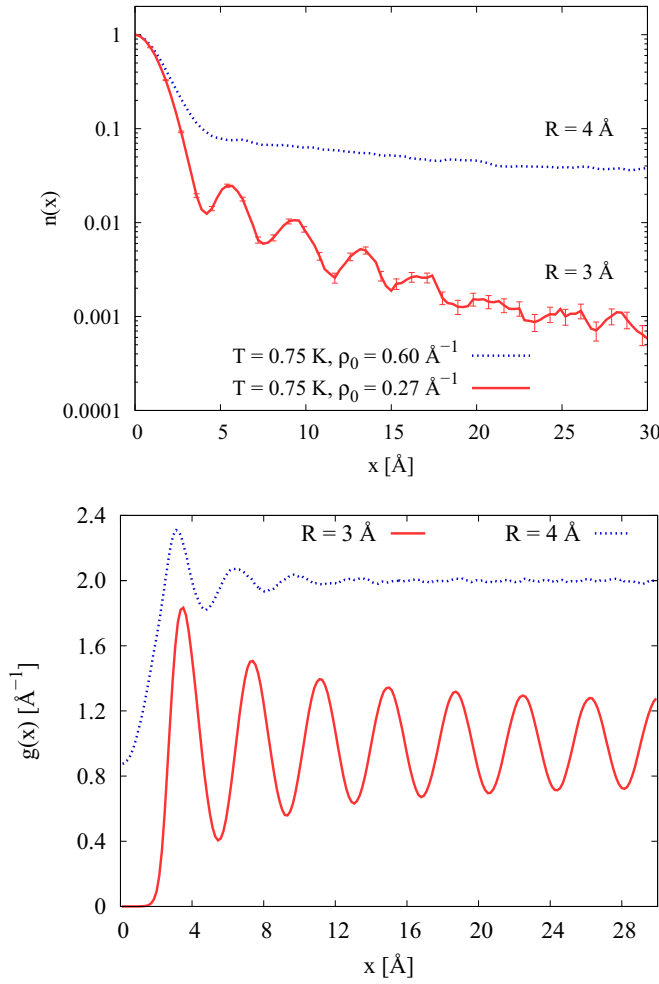
FIG. 7. Comparison of liquid ^{4}He at bulk liquid density, $\rho' = 0.0212$ Å^{-3}, confined in a nanopore of liquid radius $R = 3$ and 4 Å. In the $R = 3$ Å nanopore, where the ^{4}He forms a 1D line and is 1D at all densities, both the OBDM $n(x)$ (top) and the pair distribution function $g(x)$ (bottom) show long-range oscillations characteristic of a 1D fluid. In the $R = 4$ Å nanopore where the ^{4}He forms a cylindrical film at density $\rho' = 0.0212$ Å^{-3}, the $n(x)$ has a smooth algebraic tail and $g(x)$ has short-range oscillations characteristic of a 2D fluid.

the KT relations are used to calculate ρ_S/ρ_0 for $L \to \infty$. From the ρ_S/ρ_0 for $L \to \infty$, T_c is determined from the universal "jump" relation for ρ_S/ρ_0 at T_c,

$$\frac{\rho_S(T_c)}{\rho_0} = \frac{2m}{\hbar^2}\frac{k_B T_c}{\pi \rho}, \qquad (2)$$

where ρ is the 2D density of liquid ^{4}He in the nanopore given below in Eq. (A3). A further description of this procedure applied to the present films appears in the Appendix.

Figure 10 shows the PIMC superfluid fraction ρ_S/ρ_0 versus temperature T of liquid ^{4}He at density $\rho_0 = 0.4$ Å^{-1} calculated for several lengths L of the nanopore. The solid lines are the best fit of the ρ_S/ρ_0 calculated using the KT recursion relations for that L. Two parameters in the recursion relations are adjusted at each L. The fits are good and the parameters vary smoothly with L. The dashed line shows the
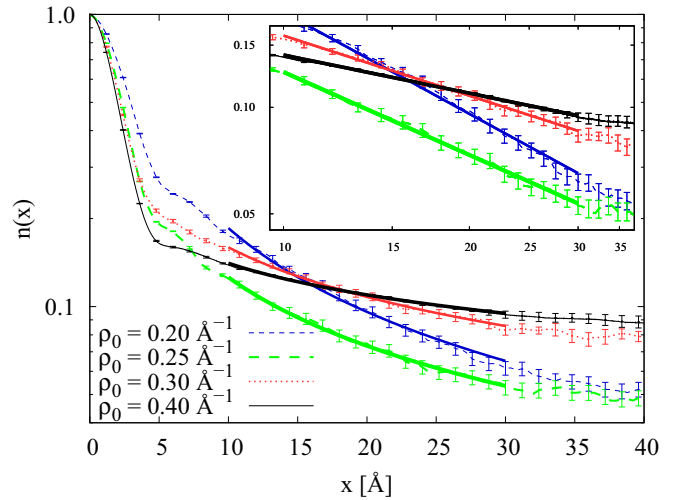

FIG. 8. One-body density matrix (OBDM) $n(x)$ of liquid ^{4}He in a nanopore of radius $R = 4$ Å for linear densities $0.20 < \rho_0 < 0.40$ Å^{-1} and $T = 0.3$ K. The height of the long-range tail of $n(x)$ increases with increasing linear density, indicating an increase in 2D character of the OBDM as density increases. The inset shows $n(x)$ in the log-log scale for better visibility of algebraic scaling in the intermediate range.

calculated ρ_S/ρ_0 for L extrapolated to $L \to \infty$. The solid line shows $(2m/\hbar^2)k_B T/(\pi \rho)$. The dashed and solid lines cross, satisfying Eq. (2) at $T_c \simeq 0.20$ K. In addition to the usual uncertainty of this method, there is an additional uncertainty introduced by using the KT recursion relations for a flat film to describe the present cylindrical-shaped films [47]. Within precision, the ρ_S/ρ_0 at $\rho_0 = 0.4$ Å^{-1} is consistent with a 2D liquid that has a low but finite $T_c \simeq 0.20$ K, in
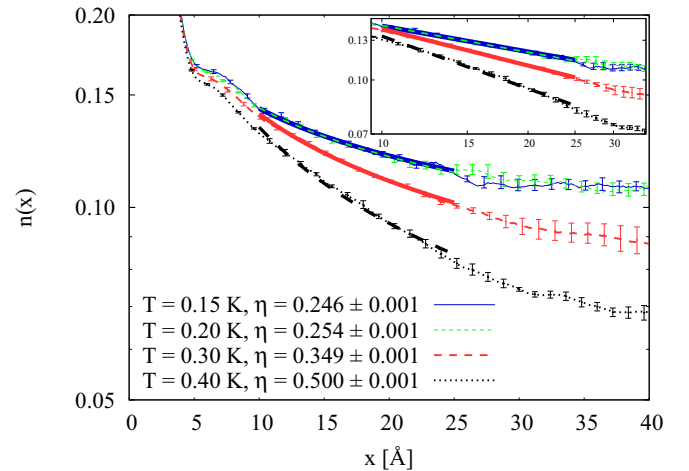

FIG. 9. OBDM $n(x)$ of liquid ^{4}He in a nanopore of radius $R = 4$ Å at linear density $\rho_0 = 0.4$ Å^{-1} showing the increase in the height of the long range as temperature decreases. The aim is to identify the temperature at which $n(x) \sim x^{-\eta}$ with $\eta = 0.25$ fits the data. This temperature is T_c. The fits suggest a $T_c \simeq 0.18$ K in liquid ^{4}He at a density $\rho_0 = 0.4$ Å^{-1} in the nanopore. The inset shows $n(x)$ in the log-log scale for better visibility of algebraic scaling in the intermediate range.
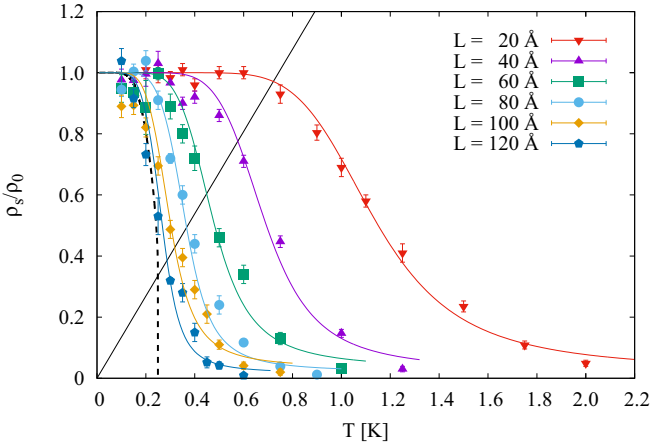
FIG. 10. Plot of ρ_S/ρ_0 vs T for samples of several lengths L at linear density $\rho_0 = 0.4$ Å^{-1}. The colored solid lines are fits of the Kosterlitz-Thouless (KT) recursion relations to PIMC ρ_s/ρ_0 (data points). The black dashed line is ρ_s/ρ_0 extrapolated to $L \to \infty$ using the KT relations. The solid line is $k_B T/(\pi \rho \hbar/2m)$ from Eq. (2). The black lines cross at $T_c \simeq 0.20$ K which is in agreement with the T_c determined from the OBDM.

agreement with $T_c = 0.15$–0.20 K predicted from the OBDM using Kosterlitz-Thouless theory.

V. DISCUSSION

We have illustrated a crossover from 1D to 2D in an accurate model of liquid ^{4}He confined in a nanopore of liquid radius $R = 4$ Å. The nanopore wall in the model represents the nanopore and the solid ^{4}He layers on the nanopore walls so that the liquid is confined to $R = 4$ Å. The equilibrium configuration of the liquid is a low-density, 1D line of liquid along the centerline of the nanopore. There is a significant distribution of liquid around the 1D centerline at equilibrium. The equilibrium linear density in the nanopore is $\rho_0 = 0.15$ Å^{-1}, similar to that of a freestanding line of 1D ^{4}He. As pressure is applied, the density in the line increases and there is a gradual crossover of ^{4}He from a 1D line to a 2D film. The film lies roughly midway between the centerline and the pore wall. At higher density all of the ^{4}He lies in the 2D film. In this way, there is a crossover from 1D to 2D as a function of pressure without changing the confining boundaries of the nanopore.

The location of the ^{4}He in the nanopore is determined chiefly by the hard core of the ^{4}He - ^{4}He potential (hard-core diameter $\sigma \simeq 2.5$ Å) and that of the nanopore wall. The center of a ^{4}He atom cannot approach the nanopore wall closer than $\sigma/2 \simeq 1.25$ Å, as seen from the ^{4}He distributions shown in Fig. 3. The effective volume accessible to the liquid ^{4}He is $V \simeq \pi (R - 1)^2 L$ Å^{-3}. The minimum energy configuration, a dilute 1D line of ^{4}He peaked at the pore center, minimizes the ^{4}He - ^{4}He and ^{4}He-wall contact. As pressure is applied and the ^{4}He - ^{4}He spacing in the line decreases, there is a crossover to a 2D film where the ^{4}He - ^{4}He spacing can be larger. The film lies roughly 2 Å from the pore wall to minimize hard-wall contacts.

The dimensions of the fluid were determined chiefly from the character and scaling of the superfluid fraction ρ_S/ρ_0,

the OBDM $n(x)$, and the pair correlation function $g(x)$. The 1D character at low densities is most clearly seen in ρ_S/ρ_0 and $g(x)$. Specifically, ρ_S/ρ_0 was calculated using the general relation derived by Pollock and Ceperley [48] expressing ρ_S/ρ_0 in terms the number W of paths winding around the sample. For 1D this relation is

$$\frac{\rho_S}{\rho_0} = \left(\frac{TL}{\sigma \rho_0}\right)\langle W^2 \rangle = \alpha_0 \langle W^2 \rangle, \qquad (3)$$

where T is the temperature, L is the length of the sample, $\sigma = \hbar^2/k_B m = 12.1193$ K Å^2, and $\alpha_0 \equiv (TL/\sigma \rho_0)$. The expectation value of W was calculated using PIMC methods [9,10,45]. The 1D expression for ρ_S/ρ_0 was used at all densities.

If the fluid is a 1D LL, ρ_S/ρ_0 is again given by Eq. (3) but the expectation value of W can be obtained from the LL expression [24],

$$\langle W^2 \rangle = \sum_W W^2 e^{-\frac{1}{2}\alpha W^2} \Big/ \sum_W e^{-\frac{1}{2}\alpha W^2}, \qquad (4)$$

where

$$\alpha = \left(\frac{\pi k_B T L}{\hbar v_J}\right) = \alpha_0 \left(\frac{v_J}{v_J^0}\right)^{-1}, \qquad (5)$$

and v_J is the kinetic LL parameter. For a uniform 1D Bose liquid, as investigated in the present paper, v_J should reduce to the uniform LL value, $\hbar v_J^0 = \pi (\hbar^2/m)\rho_0$.

We fitted the LL expression for ρ_S/ρ_0 with $\langle W^2 \rangle$ given by Eq. (4) to the PIMC ρ_S/ρ_0 calculated directly from Eq. (3) with v_J treated as a free fit parameter. At low density, up to $\rho_0 = 0.30$ Å^{-1}, the fit is good, as shown in Fig. 3. Also, the best fit is obtained when $v_J = v_J^0$, as predicted by LL theory. Thus ρ_S/ρ_0 clearly shows LL character at low density. At higher density, $\rho_0 \gtrsim 0.30$ Å^{-1}, the fit is not good. Similarly, at low density, $g(x)$ is zero, or close to zero, at small x up to a hard-core diameter $\sigma \simeq 2.5$ Å, as expected for a 1D line of liquid.

At high density, both $g(x)$ and the OBDM show 2D character. The OBDM has a long-range tail characteristic of 2D. Both $g(x)$ and the OBDM are smooth at long range. They do not oscillate with x as found in a 1D LL at high density. The 2D character at high density is most clearly seen in the temperature dependence of the OBDM. The slope of the long-range tail with x decreases with decreasing temperature, as expected for 2D. The slope reaches the value predicted for a superfluid transition in 2D at $T_c \simeq 0.15$–0.20 K. The ρ_S/ρ_0 is consistent with this low T_c. Thus the liquid at high density is characteristic of a 2D liquid with a low but finite T_c.

It is interesting that although there is a distribution of ^{4}He around the centerline at low density, the liquid still shows 1D LL character. For example, at $\rho_0 = 0.30$ Å^{-1}, where there is a significant density distribution perpendicular to the nanopore, the PIMC calculated ρ_S/ρ_0 is still well fitted by the LL ρ_S/ρ_0, as well as at lower density (see Fig. 3). This suggests that a distribution perpendicular to the 1D line does not destroy the 1D character. This could be helpful in creating systems experimentally that show 1D character. Also, a Hubbard model of 1D places all density (particles) exactly on a line.

The present results suggest that this approximation at least will continue to be valid for systems that have a distribution of density around the 1D line. It would be interesting to test how large a distribution of atomic density perpendicular to the 1D line is possible in a system before the system loses its 1D character. Equally, it is interesting that the crossover from 1D to 2D is in the linear density range $\rho_0 = 0.30$–0.40 Å^{-1}. It is in this range that the distribution perpendicular to the 1D line develops a film character (see Fig. 3). Thus, apparently a distribution characteristic of the second dimension is needed to obtain a crossover to that dimension.

The T_c obtained above for a dilute, single 2D film is very low, $T_c \simeq 0.15$–0.20 K. In previous PIMC calculations [27] for larger diameter pores where there were two to three layers of liquid at higher liquid densities, we obtained significantly higher values of T_c, e.g., $T_c = 1.43$ K for $R = 9$ Å^{-1}, $T_c = 1.21$ K for $R = 7.3$ Å, and $T_c \sim 0.3$–0.7 K for $R = 6$ Å. Wada *et al.* [49] and Taniguchi *et al.* [50] report observed values of $T_c = 1.0$ K and $T_c = 0.9$ K, respectively, for liquid at SVP in an FSM-16 nanopore of diameter $d = 28$ Å ($R = 9$ Å). It would be interesting to investigate both the density and pore size dependence of T_c to determine where $T_c \to 0$ as an indicator of where the crossover to 1D is located in nanopores. Equally, it would be interesting to investigate the flow [51,52] and dynamics [53] of liquid ^{4}He in smaller pore media to reveal the 1D character.

ACKNOWLEDGMENTS

APPENDIX

In order to determine the superfluid transition temperature, we have started from the KT recursion equations [40], which were originally introduced for flat films of area L^2,

$$\frac{dK^{-1}(l)}{dl} = 4\pi^3 y^2(l), \tag{A1}$$

$$\frac{dy(l)}{dl} = [2 - \pi K(l)]y(l), \tag{A2}$$

where $K(l) = \hbar^2 \rho_S(l)/mkT$. Equations (A1) and (A2) are then integrated from 0 to $l \equiv \ln(r/d) = \ln(L/2d)$, using initial values $K(l = 0) = \hbar^2 \rho/mkT$, where ρ is the film density and $y(l = 0) = \exp(-\beta E_c)$. Since the film is cylindrical, we have calculated its density as

$$\rho = \frac{\rho_0}{2\pi r}, \tag{A3}$$

where $\rho_0 = 0.4$ Å^{-1} is the linear density and r is estimated as the average separation from the axis, $r = 1.747$ Å. KT equations are then solved numerically for different combinations of parameters d and E_c and fitted to PIMC results. The lines presented in Fig. 10 are obtained using d and E_c parameters which best fit the data. They depend on L, but E_c converges as L is increased, to 0.49 ± 0.015 K. Using this value, and taking the limit of $l \to \infty$ ($L \to \infty$) we obtained ρ_s/ρ_0 given by the dashed line in Fig. 10. The universal jump line, determined by Eq. (2), which is drawn from the origin, crosses the dashed line at $T_c = 0.245$ K. This is also the point at which ρ_s/ρ_0 becomes perpendicular to the x axis, demonstrating the jump of superfluid density from zero to finite value at the transition temperature.

Clearly, the estimations of the parameters in KT equations are approximate and the cylindrical geometry introduces additional effects, e.g., the areal density depends on the value of r used in Eq. (A3), and the shape of the density profile. In order to test the sensitivity to the value of r, we have also used the values $r = \langle r_\perp \rangle \pm \sqrt{\langle r_\perp^2 \rangle - \langle r_\perp \rangle^2} = 1.747 \pm 0.45$ Å, giving the density of $\rho = 0.039 \pm 0.01$ Å^{-2}. However, this resulted in a small change of T_c, only ± 0.005 K.

[1] S. N. Bose, Z. Phys. **26**, 178 (1924).

[2] A. Einstein, Sitzungsber. Kgl. Preuss. Akad. Wiss., Phys. Math. Kl. **22**, 261 (1924).

[3] F. London, Nature (London) **141**, 643 (1938).

[4] F. London, *Superfluids, Vol. 1: Macroscopic Theory of Superconductivity* (Wiley, New York, 1950).

[5] F. London, *Superfluids, Vol. 2: Macroscopic Theory of Superfluid Helium* (John Wiley and Sons, Inc., New York, 1954).

[6] O. Penrose and L. Onsager, Phys. Rev. **104**, 576 (1956).

[7] J. Wilks, *The Properties of Liquid and Solid Helium* (Clarendon Press, Oxford, UK, 1967).

[8] A. J. Leggett, *Quantum Liquids: Bose Condensation and Cooper Pairing in Condensed Matter Systems* (Oxford University Press, Oxford, UK, 2006).

[9] D. M. Ceperley, Rev. Mod. Phys. **67**, 279 (1995).

[10] M. Boninsegni, N. Prokof'ev, and B. Svistunov, Phys. Rev. Lett. **96**, 070601 (2006).

[11] J. M. Kosterlitz and D. J. Thouless, J. Phys. C: Solid State **6**, 1181 (1973).

[12] D. R. Nelson and J. M. Kosterlitz, Phys. Rev. Lett. **39**, 1201 (1977).

[13] F. D. M. Haldane, Phys. Rev. Lett. **47**, 1840 (1981).

[14] T. Giamarchi, *Quantum Physics in One Dimension* (Oxford University Press, Oxford, UK, 2004).

[15] D. J. Bishop and J. D. Reppy, Phys. Rev. Lett. **40**, 1727 (1978).

[16] J. D. Reppy, J. Low Temp. Phys. **87**, 205 (1992).

[17] G. A. Csáthy, J. D. Reppy, and M. H. W. Chan, Phys. Rev. Lett. **91**, 235301 (2003).

[18] N. Wada, J. Taniguchi, H. Ikegami, S. Inagaki, and Y. Fukushima, Phys. Rev. Lett. **86**, 4322 (2001).

[19] N. Wada, Y. Minato, T. Matsushita, and M. Hieda, J. Low Temp. Phys. **162**, 549 (2011).

[20] K. Yamamoto, H. Nakashima, Y. Shibayama, and K. Shirahama, Phys. Rev. Lett. **93**, 075302 (2004).

[21] K. Yamamoto, Y. Shibayama, and K. Shirahama, Phys. Rev. Lett. **100**, 195301 (2008).

[22] M. A. Cazalilla, R. Citro, T. Giamarchi, E. Orignac, and M. Rigol, Rev. Mod. Phys. **83**, 1405 (2011).

[23] A. Imambekov, T. L. Schmidt, and L. I. Glazman, Rev. Mod. Phys. **84**, 1253 (2012).

[24] A. Del Maestro and I. Affleck, Phys. Rev. B **82**, 060515(R) (2010).

[25] A. Del Maestro, M. Boninsegni, and I. Affleck, Phys. Rev. Lett. **106**, 105303 (2011).

[26] B. Kulchytskyy, G. Gervais, and A. Del Maestro, Phys. Rev. B **88**, 064512 (2013).

[27] L. V. Markić and H. R. Glyde, Phys. Rev. B **92**, 064510 (2015).

[28] L. Vranješ Markić, H. Vrcan, Z. Zuhrianda, and H. R. Glyde, Phys. Rev. B **97**, 014513 (2018).

[29] E. Krotscheck and M. D. Miller, Phys. Rev. B **60**, 13038 (1999).

[30] G. Bertaina, M. Motta, M. Rossi, E. Vitali, and D. E. Galli, Phys. Rev. Lett. **116**, 135302 (2016).

[31] K. A. Matveev and A. V. Andreev, Phys. Rev. Lett. **121**, 026803 (2018).

[32] M. C. Gordillo and D. M. Ceperley, Phys. Rev. Lett. **85**, 4735 (2000).

[33] M. Boninsegni, Phys. Rev. Lett. **111**, 235303 (2013).

[34] M. Rossi and F. Ancilotto, Phys. Rev. B **94**, 100502(R) (2016).

[35] T. Omiyinka and M. Boninsegni, Phys. Rev. B **93**, 104501 (2016).

[36] G. Ferré, M. C. Gordillo, and J. Boronat, Phys. Rev. B **95**, 064502 (2017).

[37] A. Del Maestro and M. Boninsegni, Phys. Rev. B **95**, 054517 (2017).

[38] A. J. Vidal, G. E. Astrakharchik, L. Vranješ Markić, and B. Jordi, New J. Phys. **18**, 055013 (2016).

[39] M. Boninsegni and S. Moroni, J. Low Temp. Phys. **118**, 1 (2000).

[40] D. M. Ceperley and E. L. Pollock, Phys. Rev. B **39**, 2084 (1989).

[41] P. A. Whitlock, G. V. Chester, and M. H. Kalos, Phys. Rev. B **38**, 2418 (1988).

[42] R. A. Aziz, F. R. W. McCourt, and C. C. K. Wong, Mol. Phys. **61**, 1487 (1987).

[43] J. Boronat and J. Casulleras, Phys. Rev. B **49**, 8920 (1994).

[44] J. Casulleras and J. Boronat, Phys. Rev. B **52** 3654 (1995).

[45] M. Boninsegni, N. V. Prokof'ev, and B. V. Svistunov, Phys. Rev. E **74**, 036701 (2006).

[46] M. C. Gordillo and J. Boronat, J. Low Temp. Phys. **157**, 296 (2009).

[47] V. Kotsubo and G. A. Williams, Phys. Rev. B **33**, 6106 (1986).

[48] E. L. Pollock and D. M. Ceperley, Phys. Rev. B **36**, 8343 (1987).

[49] N. Wada, Y. Minato, T. Matsushita, and M. Hieda, J. Phys. Soc. Jpn. **77**, 111012 (2008).

[50] J. Taniguchi, Y. Aoki, and M. Suzuki, Phys. Rev. B **82**, 104509 (2010).

[51] M. Savard, C. Tremblay-Darveau, and G. Gervais, Phys. Rev. Lett. **103**, 104502 (2009).

[52] M. Savard, G. Dauphinais, and G. Gervais, Phys. Rev. Lett. **107**, 254501 (2011).

[53] J. Bossy, J. Ollivier, and H. R. Glyde, Phys. Rev. B **99**, 165425 (2019).